PERGAMON

International Journal of Heat and Mass Transfer 44 (2001) 4359–4367

International Journal of HEAT and MASS TRANSFER

www.elsevier.com/locate/ijhmt

Spatial development of disturbances in plane Poiseuille flow: a direct numerical simulation using a commercial CFD code

J. Severin [a], K. Beckert [a], H. Herwig [b,*]

[a] *Technische Thermodynamik, TU Chemnitz, D-09107 Chemnitz, Germany*
[b] *Technische Thermodynamik, TU Hamburg-Harburg, D-21073 Hamburg, Germany*

Received 26 May 2000; received in revised form 2 November 2000

Abstract

Spatial development of small amplitude disturbances in plane Poiseuille flow is investigated numerically using a commercial CFD code (CFX 4.2). Small amplitude Tollmien–Schlichting (TS) waves known from an Orr–Sommerfeld analysis are superimposed as initial conditions on a fully developed laminar channel flow. The downstream spatial disturbances are calculated on the basis of the full Navier–Stokes equations (NSE). Results are compared to calculations based on the Orr–Sommerfeld equations (OSE). In a second step the thermal energy equation is solved in addition to the NSE to investigate the temperature effects and especially the development of temperature disturbances. A certain delay in the development of these disturbances is found which is due to a *thermal receptivity* mechanism. These results again are compared to OSE calculations.

Keywords: Flow; Numerical methods; Stability

1. Introduction

The laminar-turbulent transition process is often initiated by an amplification of small disturbances. The small disturbance linear stability theory, based on the famous Orr–Sommerfeld equation (OSE), is a mathematical tool for analysing the initial stage of the transition process. It provides certain stability criteria in terms of threshold values of the Reynolds number and amplification rates for the disturbances. According to these criteria the flow is unstable if the amplification is positive, which may occur if the Reynolds number exceeds a critical value Re_c. For plane Poiseuille flow the critical Reynolds number based on half the channel height $h^* = H^*/2$ and the centreline velocity U_c^* is $Re_c = U_c^* h^*/\nu^* = 5772$.

In the Orr–Sommerfeld theory a parallel flow is assumed, i.e., changes of the disturbance amplitude functions and of the mean flow in the downstream direction are neglected. Thus the theory provides a local analysis, i.e., the flow history or upstream effects from an outflow boundary are not included.

Since this theory is only a first step in the direction of a complete analysis there have been many extensions of the OSE-theory during the last decades. In today's stability investigations non-parallel as well as non-linear or variable property effects are points of particular interest (see [1] or [2] for a review).

With all these effects included in the mathematical models (which are all deduced from the Navier–Stokes equations (NSE)) one gets closer and closer to the full equations. With the fast development of computer technology the trend will be to solve the NSE themselves even for the analysis of flow stability characteristics. Though this sounds like a progress per se, one should always keep in mind that deducing mathematical models from the full NSE goes hand in hand with an understanding of the physics of the problem. This, however, might get lost by attacking the full equations.

From these considerations we conclude that in the future stability analysis may be routinely based on the full NSE, that, however, a critical interpretation based on physical considerations is absolutely necessary.

* Corresponding author. Tel.: 49-40-428783044; fax: 49-40-428784169.

E-mail address: h.herwig@tu-harburg.de (H. Herwig).

0017-9310/01/$ - see front matter
PII: S0017-9310(01)00074-6

Nomenclature

a^*	physical quantity
A	amplitude
$\vec{B}^*$	body force
c_p^*	specific heat
h^*, H^*	channel height
h^*, H^*	enthalpy, total enthalpy
L^*	length
p^*	pressure
Pr	Prandtl number
Re	Reynolds number
S^*	source term
t^*	time
T^*	temperature
u^*, v^*	velocity components
$\vec{U}^*$	velocity vector
x^*, y^*, z^*	Cartesian coordinates

Greek symbols

$\hat{\alpha}$	stability parameter
λ^*	thermal conductivity
μ^*	dynamic viscosity
ν^*	kinematic viscosity
ρ^*	density
σ^*	stress tensor
Θ	dimensionless temperature
ω	dimensionless frequency

Subscripts

c	critical value, centreline, computation domain
i	imaginary part
r	real part
v	v-velocity
T	temperature

Superscripts

*	dimensional quantity
$'$	disturbance quantity, derivative
$\bar{}$	mean flow quantity
$\hat{}$	complex quantity

In our study, we want to find out to what extent commercial CFD codes can be used today already for a direct numerical simulation (DNS) of flow stability characteristics. Plane Poiseuille flow is a "good candidate" since its mean flow is a parallel flow. Moreover, the analytical parabolic velocity profile is an exact solution of the full NSE. Thus the Orr–Sommerfeld analysis, which we want to use as a reference theory, is an exact description of the linear stability behaviour of (exponentially) small disturbances.

In previous studies like those by Fasel and Bestek [3] or Chung et al. [4] the stability of plane Poiseuille flow was analysed by DNS codes especially developed for these purposes. Instead, we want to use the commercial CFD code CFX 4.2 by the AEA Technology to investigate the stability of a channel flow. Our special interest is focused on grid dependence, computing time and accuracy.

Since a spatial simulation of the problem under investigation needs a great amount of computer recourses most studies have been performed in terms of a temporal simulation with periodic boundary conditions in the mean flow direction. The computation domain then only has to be a multiple of the wavelength of the investigated TS wave. In the unstable parameter domain the numerical errors, always present in the calculations, will automatically lead to an amplified disturbance and finally to self-sustained oscillations [5]. For non-periodic flows, however, this method is not applicable. Such flows must be investigated using a spatial mode analysis. In what follows we therefore analyse the spatial development of Tollmien–Schlichting (TS) waves.

2. Numerical models

2.1. NSE model

The basic setup of the problem is relatively simple and a sketch of it is shown in Fig. 1. Our computational domain is the rectangle A–B–C–D. We assume the flow to be fully developed, two-dimensional and incompressible. The basic equations solved by the program CFX 4.2 are the well-known conservation equations for mass, momentum and, in the non-isothermal case, energy (see the CFX manual for details)

$$\frac{\partial \rho^*}{\partial t^*} + \nabla^*(\rho^* \vec{U}^*) = 0, \tag{1}$$

$$\frac{\partial \rho^* \vec{U}^*}{\partial t^*} + \nabla^*(\rho^* \vec{U}^* \otimes \vec{U}^*) = \vec{B}^* + \nabla^* \cdot \sigma^*, \tag{2}$$

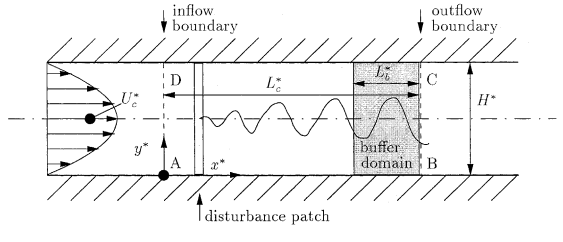

Fig. 1. Sketch of the channel flow and the computation domain for the NSE calculation.

$$\frac{\partial \rho^* H^*}{\partial t^*} + \nabla^*(\rho^* \vec{U}^* H^*) - \nabla^* \cdot (\lambda^* \nabla^* T^*) = \frac{\partial p^*}{\partial t^*}. \quad (3)$$

Here $\vec{U}^*$ is the velocity vector, p^* the pressure, T^* the temperature, t^* the time, ρ^* the density, λ^* the thermal conductivity and H^* the total enthalpy $H^* = h^* + \vec{U}^{*2}/2$. The stress tensor is $\sigma^* = -p^*\delta + \mu^*(\nabla^*\vec{U}^* + (\nabla^*\vec{U}^*)^{\mathrm{T}})$ with the molecular viscosity μ^*. In Eq. (2) $\vec{B}^*$ is a body force.

The boundary conditions are no slip at the lower and upper walls. The inflow boundary condition at A–D is the fully developed velocity profile. Since there are no special boundary conditions for the outflow boundary in CFX 4.2 to provide an unhindered passage of the outgoing disturbance waves we decided to use the so-called "MASS FLOW BOUNDARY" condition. For the problem under consideration this boundary condition is similar to assuming a fully developed flow at the exit B–C, which, however, will lead to a reflection of the outgoing waves and a superposition of the reflected and outgoing disturbances. This is a crucial point of the investigation and will be discussed later.

In the present study, the disturbances were introduced at some location downstream of the inflow boundary, on the "disturbance patch" ($x^* = x^*_{\mathrm{dp}}$). Therefore, first the Orr–Sommerfeld solution for a given disturbance frequency and Reynolds number was calculated to get the amplitude functions of the $v^{*\prime}$ and $u^{*\prime}$-components of the disturbance (see next paragraph). Then the two-dimensional TS wave (only the $v^{*\prime}$-component)

$$v^{*\prime}(x^* = x^*_{\mathrm{dp}}, y^*, t^*) = A\ \mathrm{Real}\left(\hat{v}^* \exp(-\mathrm{i}\omega^* t^*)\right) \quad (4)$$

was superimposed on the laminar parabolic velocity profile. Here, A is the amplitude of the TS wave, $\hat{v}^*$ the dimensional amplitude function calculated from the OSE and ω^* the corresponding frequency. Since CFX 4.2 does not provide direct access to the velocity field during the iteration process we had to model the disturbances on the disturbance patch by using source terms. This procedure is described in detail in the CFX manual. It is based on the fact that in the linearised form all transport equations can be written as

$$\text{convection} - \text{diffusion} = \text{sources}. \quad (5)$$

For example, the source term for the $v^{*\prime}$ component in the momentum equation then reads

$$S^*_{\mathrm{v}} = A \sin(\omega^* t^*)\,\mathrm{Real}\left(\hat{v}^*(y^*)\right). \quad (6)$$

CFX 4.2 provides many performance parameters like the choice of a differencing scheme, number of inner/outer iterations, pressure coupling algorithm (SIMPLE/SIMPLEC) and many more. The default parameter settings were used in all our calculations, except for the differencing scheme, where quadratic upwind differencing (QUICK) instead of hybrid differencing was used.

Though the equations are given in a dimensional form they can be treated like non-dimensional equations by a special choice of the length ($H^* = 1$ m), the density ($\rho^* = 1$ kg/m^3) and the viscosity ($\mu^* = 10^{-4}$ kg/ms; 10^{-4} is preferred to 1 in order to get numbers of order one in the results). Thus they are only formally like dimensional equations.

During some test calculations the results were found to be very sensitive to time step variations. Finally, $\Delta t^* = 0.01$ s was taken as the choice for the best accuracy. Simple rectangular equidistant grids of size 1001×51 to 2501×121 were tested depending on the geometrical size of the channel ($L^* = 25$ m/35 m, $H^* = 2h^* = 1$ m). More details will be given in the results and discussion part below.

2.2. OSE model

Solutions of the OSE serve as reference solutions. The OSE can easily be deduced from the full NSE by decomposing all flow quantities into a mean part $\bar{a}^*(y^*)$ and a disturbance part $a^{*\prime}(x^*, y^*, t^*)$. Assuming the disturbance part to be of the wave-like form (spatial analysis)

$$a^{*\prime}(x^*, y^*, t^*) = \hat{a}^*(y^*) \exp(\mathrm{i}\hat{\alpha}^* x^* - \mathrm{i}\omega^* t^*) + \text{c.c.} \quad (7)$$

and non-dimensionalising all quantities with respect to half the channel height $h^* = H^*/2$ and the centreline velocity U^*_{c} we get the OSE in $u - v$ form

$$\mathrm{i}\hat{\alpha}\hat{u} + \hat{v}' = 0, \quad (8)$$

$$(\mathrm{i}\hat{\alpha}\bar{u} - \mathrm{i}\omega)[\hat{u}' - \mathrm{i}\hat{\alpha}\hat{v}] + \bar{u}''\hat{v} + \frac{1}{Re}\left(\hat{u}''' - \hat{\alpha}^2\hat{u}' - \mathrm{i}\hat{\alpha}\hat{v}'' + \mathrm{i}\hat{\alpha}^3\hat{v}\right) = 0. \quad (9)$$

For the non-isothermal case the disturbance thermal energy equation is deduced likewise from the full energy equation

$$(\mathrm{i}\hat{\alpha}\bar{u} - \mathrm{i}\omega)\hat{\Theta} + \bar{\Theta}'\hat{v} - \frac{1}{RePr}(\hat{\Theta}'' - \hat{\alpha}^2\hat{\Theta}) = 0. \quad (10)$$

Here $Re = \rho^* U^*_{\mathrm{c}} h^*/\mu^*$ is the Reynolds number, $Pr = \mu^* c^*_{\mathrm{p}}/\lambda^*$ the Prandtl number with the heat capacity c^*_{p}.

For our investigation two different flow situations shown in Fig. 2 were chosen as test cases. One is a subcritical case with $Re = 5000$; the second is a supercritical flow with $Re = 10\,000$. In the subcritical case the frequency is $\omega = \omega^* h^*/U^*_{\mathrm{c}} = 0.3302$, and in the supercritical case it is $\omega = 0.2375$. The corresponding complex eigenvalues from the OSE calculation are $\hat{\alpha} = \hat{\alpha}^* h^* = 1.1557 + \mathrm{i}0.0106$ (subcritical case) and $\hat{\alpha} = 1.0006-$

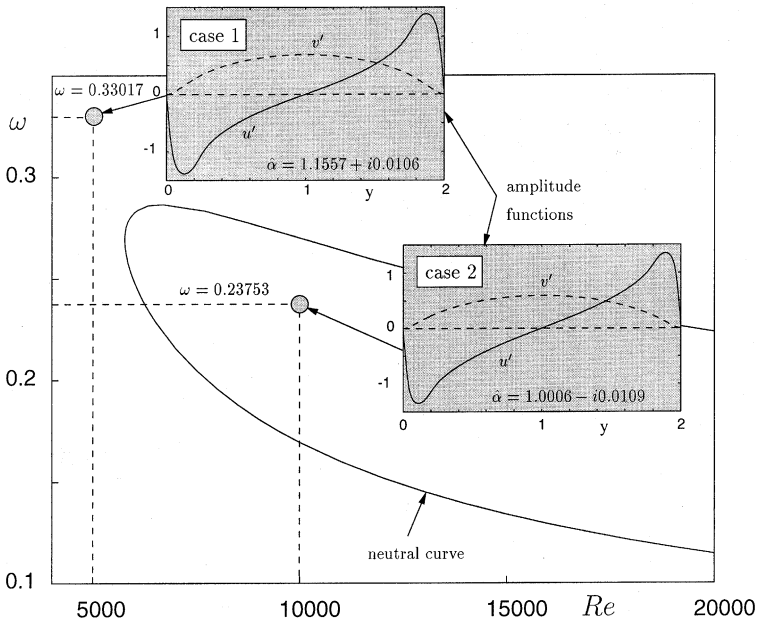

Fig. 2. Neutral curve for the channel flow (OSE solutions).

i0.0109 (supercritical case). The amplitude functions for these eigenvalues are also depicted in Fig. 2.

The programme for solving the OSE is based on a Chebyshev collocation approach combined with a regular false method for finding the eigenvalues (for details see [6]).

3. Results and discussion

In the present study, we considered the two-dimensional laminar channel flow between two plates located at $y^* = 0$ and $y^* = H^*$. At a distance of $x^* = 1.52H^*$ from the inflow boundary a disturbance of the form (4) was introduced. The computation domain is of length $25H^*$.

Fig. 3(a) shows a comparison between the NSE and OSE calculations for case 1 (see Fig. 2) (grid resolution: 1801×81). The development of the v'-component of the disturbance at the centreline in the downstream direction is shown. Due to the fact that the outgoing disturbances are reflected at the outflow boundary a wave emerges that has got a slightly different wavelength compared to the original OSE result: $\alpha_{r,NSE} = 1.2$ instead of $\alpha_{r,OSE} = 1.1557$. Next, a recalculation of the OSE was made with exactly the NSE wavelength $\alpha_r = 1.2$ in order to compare this to the original NSE result. A nearly perfect correspondence of both results is now reached, see Fig. 3(b). However, one should keep in mind that NSE results only match the OSE case which is shifted in wavelength (from 1.1557 to 1.2). Thus, the wavelength correspondence is enforced. The amplification rate, however, could be different (which it is not due to a good correspondence between NSE and OSE). The computation domain for these calculations was $L_c^* = 25H^*$.

The corresponding amplitude functions are depicted in Fig. 4. The amplitude functions shown in this figure are normalised to one at their maximum. The remaining difference in the amplitude functions u' is very small and for an increasing resolution it will go to zero.

The shift in wavelength of the disturbance due to reflection of the outgoing wave is a crucial point in this study. If only one would look at the downstream developing wave without considering the origin of it the results are perfect. Then we have an excellent agreement of the NSE solution with the OSE results. However, the mechanism that transforms the time periodic wave of the source into a spatial developing wave is different in the OSE, because the OSE does not take into account an upstream effect of the outflow boundary condition. In particular there is no outflow boundary in the OSE model. Hence our task is to adjust the NSE model to the OSE model and especially to avoid the reflection of the outgoing waves in the NSE model. Therefore, we introduced the so-called *buffer domain* in our NSE model (see [4] for this idea and more details).

In this buffer domain the governing equations are modified to enforce strictly outgoing waves. To avoid reflections the streamwise viscous terms must be set to zero. However, an ill-posed problem then causes a breakdown of the solver in CFX 4.2 so that very small but non-zero values were taken to avoid this breakdown.

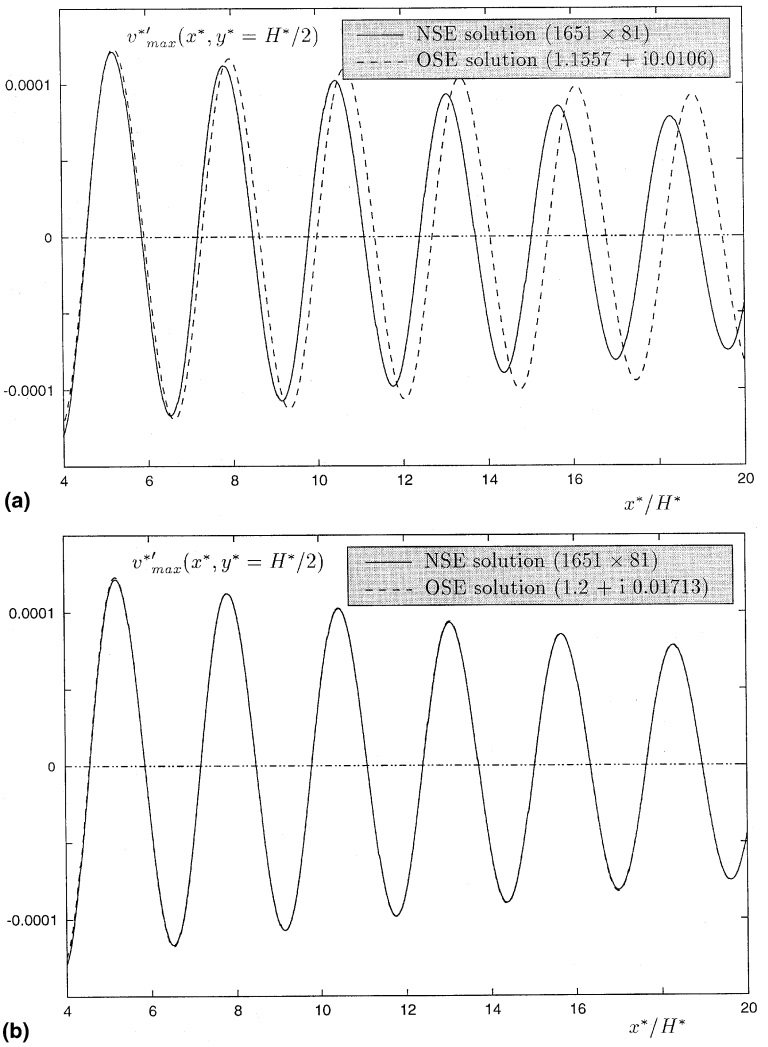

Fig. 3. $v^{*\prime}_{\max}$ at the centreline; comparison of OSE and NSE solutions for two different grid resolutions: (a) 1001×61; (b) 1651×81.

Due to the large computation time for only one simulation an optimisation of the geometric size of the buffer domain was out of reach. Its size was set to $L^*_{\mathrm{b}} = 10H^*$ as shown in Fig. 1. For the calculations with buffer domain the computation domain was then extended to $L^*_{\mathrm{c}} = 35H^*$.

The results in Fig. 5 show for case 2 (see Fig. 2) that the reflection of outgoing waves can be avoided by this procedure, like it had been demonstrated by Chung et al. [4] already. Since they, however, used their own code we thought it is worth to show that introducing a buffer domain really solves the problem, even in a "general purpose code" which is not at all tuned for solving stability problems.

NSE solutions for two different grid resolutions are compared to the corresponding OSE solution. Since for these calculations a buffer domain was introduced the time periodic wave of the source was correctly transformed to a spatial disturbance. The corresponding OSE solution (case 2: $\hat{\alpha} = 1.0006 + \mathrm{i}0.0109$) shows a good agreement with the NSE solution with respect to the wavelength. The growth rate, however, still is too low. Obviously the grid resolution is insufficient, which is shown in Fig. 6. Here the amplitude after approximately six wavelengths (see Fig. 5 for the corresponding insert) is shown as a function of $1/N_x$ with N_x being the number of grid points in the x^*-direction. Assuming the error (deviation of NSE solution from OSE results) to be proportional to $1/N_x$ there is a nearly perfect correspondence of the OSE solution with the NSE solutions for $N_x \to \infty$. For the resolution 2201×91 the growth rate is approximately $\alpha_i = 0.0005$ (OSE: 0.0109).

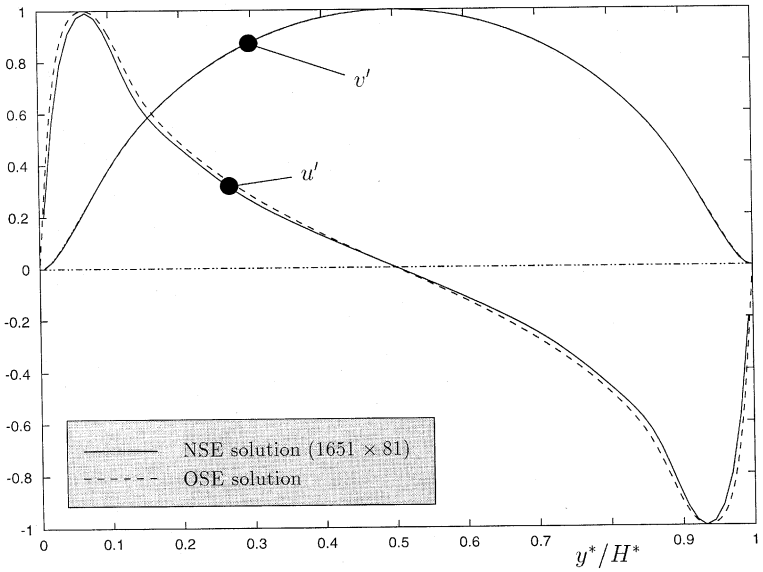

Fig. 4. Comparison of the amplitude functions from OSE and NSE solutions, case 1 (grid resolution: 1651×81).

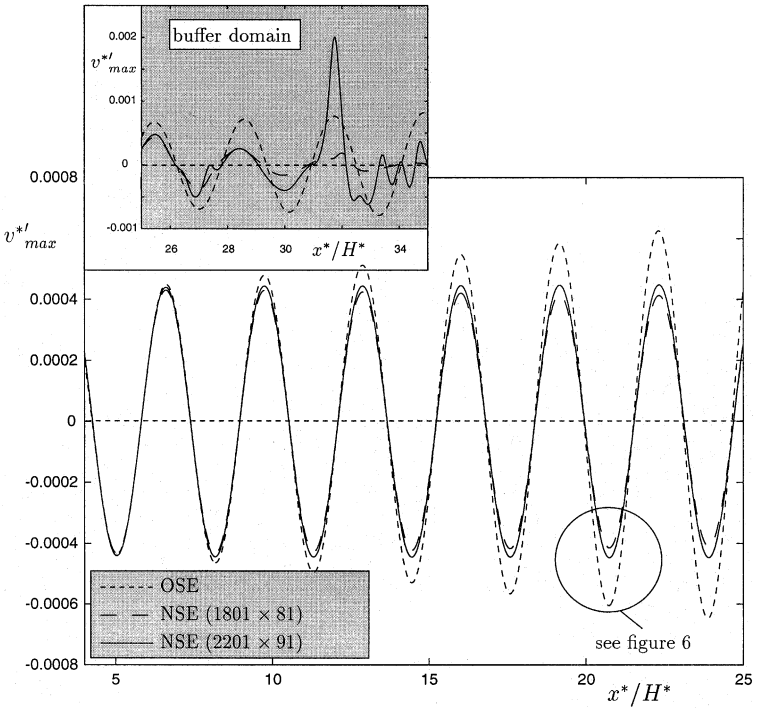

Fig. 5. $v^{*\prime}_{\max}$ at the centreline: comparison of NSE solutions (with buffer domain) with the corresponding OSE solution.

In the buffer domain (small streamwise viscous terms) unphysical results arise due to the manipulation of the equations. An example is given in the grey shaded inset in Fig. 5.

All calculations were performed on a HP 9000/889 K460 workstation cluster. A typical number of 300 time steps, each of it with four iterations and 500 s of CPU time (grid resolution: 2001×81) thus took approximately 40 h of total CPU time. Since computers with these specifications are often multi-user devices such calculations may last for days or weeks.

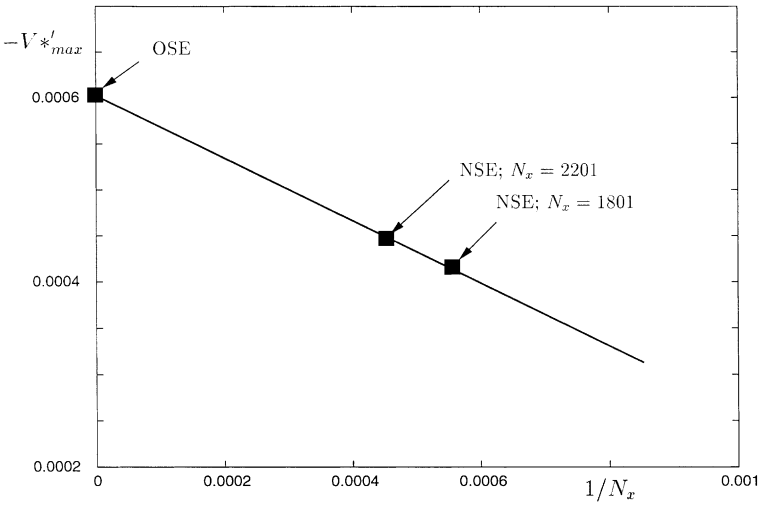

Fig. 6. Behaviour of the NSE results for $N_x \to \infty$; see Fig. 5.

3.1. Temperature disturbances

Among all studies about flow stability only very few address the problem of additional heat transfer and its effect on flow stability. This effect, however, can be large. For example, Wazzan [7] found that the critical Reynolds number of a flat plate boundary layer in water under the effect of heat transfer varies between 520 and 16 000.

Physically, heat transfer affects flow stability through the temperature dependence of the properties ρ^*, μ^*, λ^* and c_p^* (density, viscosity, thermal conductivity and specific heat). Two major effects lead to changes in the stability characteristic of a fluid: one is the action of the mean temperature field and the second is the effect of temperature fluctuations. The latter one gave rise to controversial discussion in the past. Some studies simply neglected the temperature fluctuations, like Wazzan et al. [7] for a flat plate flow or Potter and Graber [8] for the plane Poiseuille flow. Others, like the study of Schäfer and Herwig [9], for example, used the so-called shape assumption to investigate the effect of temperature disturbances, i.e., they assumed the temperature disturbances to be of the same form as the velocity disturbances. This is a good approximation as long as the stability is only of interest in the fully developed region, where the temperature disturbances already are fully developed in size and form. Due to the passive character of the temperature disturbances (they are initiated by velocity fluctuations) a certain time or length, however, is necessary for the development to their final form and size.

An investigation of Herwig and You [10] showed that the shape assumption is a useful approximation and that the delay in the development of temperature disturbances (thermal receptivity) is negligible for most stability considerations.

With the development of temperature fluctuations in mind we address two major questions: (1) Is it possible to get accurate results for the temperature disturbances with the commercial code CFX 4.2? (2) Can we observe the *thermal receptivity* mechanism described by Herwig and You [10] also in our spatial stability analysis?

In Fig. 7 the development of the amplitude of the temperature disturbance in the downstream direction is shown for a Prandtl number of $Pr = 0.7$. The grey shaded inserts show a typical downstream travelling wave of the temperature disturbance and the corresponding v-velocity disturbance at $y^* = H^*/2$. The results were calculated without a buffer domain (for a comparison see Fig. 3(b)). In agreement with the findings of Herwig and You [10] for their time mode analysis the temperature disturbance starts at the disturbance patch with zero amplitude and then grows while travelling downstream. After an overshoot a small adjustment zone follows before it reaches its final state after approximately four wavelengths comparing well with the OSE results based on the shape assumption.

In Fig. 8 disturbance amplitude functions from the NSE calculations are compared to the OSE result, which, according to the shape assumption, is the final form of the temperature disturbance amplitude function. The NSE calculations show a good agreement with the OSE result. From the beginning ($x^* = 6.0H^*$) the shape functions are close together. Near the centre of the channel the final shape (OSE result) is not reached within the calculated distance downstream. Together with Fig. 7 these results show that for temperature disturbances the size as well as the approximate shape is attained very fast (2–3 wavelengths).

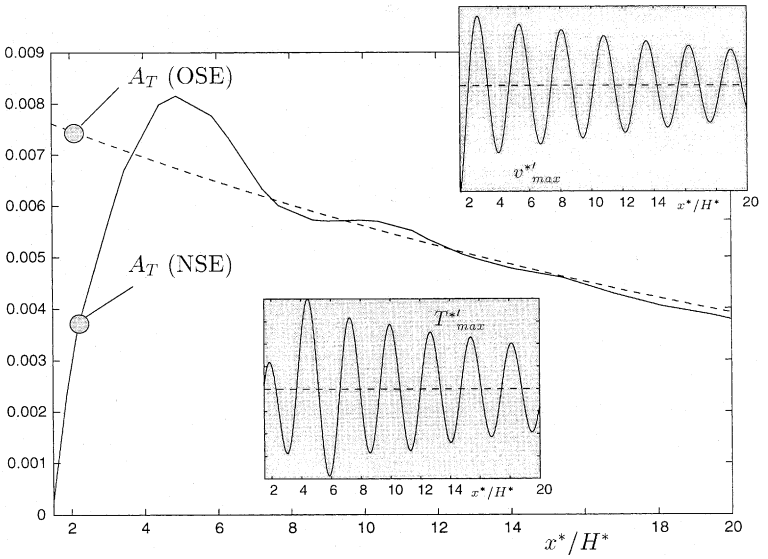

Fig. 7. Downstream development of $|T^{*\prime}_{\max}|$ (absolute value of the amplitude of $T^{*\prime}$), grid resolution: 1651×81, $Pr = 0.7$.

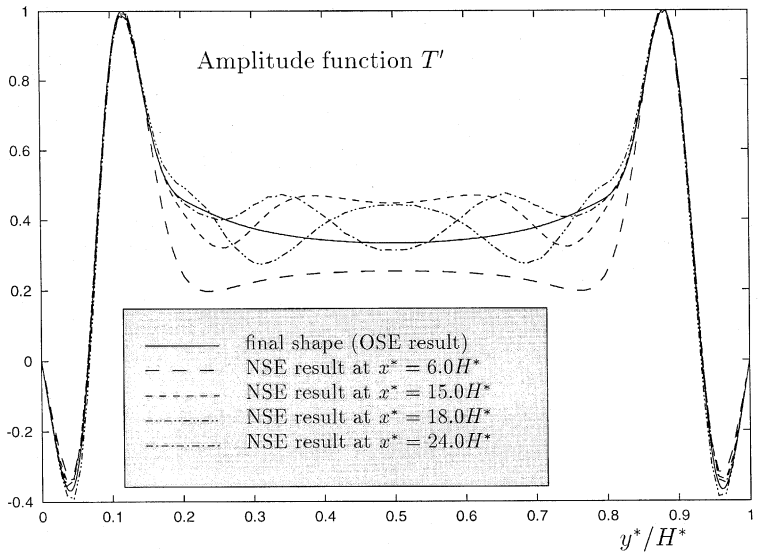

Fig. 8. Development of the amplitude function of T^*, $Pr = 0.7$.

4. Conclusions

From our numerical calculations based on the commercial CFD code CFX 4.2 we conclude that flow stability can be analysed without major modifications in the code.

However, special attention must be given to the adequate grid resolution as well as to the problem of reflecting waves.

Even with high-performance computers CPU times are very high. Though we are certainly still far away from replacing flow stability considerations based on special stability equations (derived from the NSE) by solving the NSE themselves, increasing computer performance can make this alternative more and more attractive in the future.

Acknowledgements

This project was supported by the DFG (Deutsche Forschungsgemeinschaft).

References

[1] H. Oertel Jr., J. Delfs, Strömungsmechanische Instabilitäten, Springer, Berlin, 1996.
[2] H. Schlichting, K. Gersten, Boundary Layer Theory, Springer, Berlin, 2000.
[3] H. Fasel, H. Bestek, Investigation of nonlinear, spatial disturbance amplification in plane Poiseuille flow, Institut A für Mechanik, Universität Stuttgart, Germany, 1978.
[4] Y.M. Chung, H.J. Sung, A.V. Boiko, Spatial simulation of the instability of channel flow with local suction/blowing, Phys. Fluids 9 (11) (1997) 3258–3266.
[5] P. Schäfer, Untersuchung von Mehrfachlösungen bei laminaren Strömungen, Ph.D. thesis, Ruhr-Universität Bochum, Germany, 1995.
[6] J. Severin, Der Einfluß der Wärmeübertragung auf die Stabilität von Strömungen, Ph.D. thesis, TU-Chemnitz, Germany, 1999.
[7] A.R. Wazzan, G. Keltner, T.T. Okamura, A.M.O. Smith, Spatial stability of stagnation water boundary layer with heat transfer, Phys. Fluids 15 (1972) 2114–2118.
[8] M.C. Potter, E.J. Graber Jr., Stability of plane Poiseuille flow with heat transfer, NASA TN D-6027, 1970.
[9] P. Schäfer, H. Herwig, Stability of plane Poiseuille flow with temperature dependent viscosity, Int. J. Heat Mass Transfer 36 (9) (1993) 2441–2448.
[10] H. Herwig, X. You, Thermal receptivity of unstable laminar flows with heat transfer, Int. J. Heat Mass Transfer 40 (1997) 4095–4103.